nature geoscience

LETTERS

PUBLISHED ONLINE: 10 NOVEMBER 2014 | DOI: 10.1038/NGEO2290

Termini of calving glaciers as self-organized critical systems

J. A. Åström[1], D. Vallot[2]*, M. Schäfer[3,4], E. Z. Welty[5], S. O'Neel[5,6], T. C. Bartholomaus[7], Yan Liu[8], T. I. Riikilä[9], T. Zwinger[1], J. Timonen[9,10] and J. C. Moore[2,3,8]*

Over the next century, one of the largest contributions to sea level rise will come from ice sheets and glaciers calving ice into the ocean[1]. Factors controlling the rapid and nonlinear variations in calving fluxes are poorly understood, and therefore difficult to include in prognostic climate-forced land-ice models. Here we analyse globally distributed calving data sets from Svalbard, Alaska (USA), Greenland and Antarctica in combination with simulations from a first-principles, particle-based numerical calving model to investigate the size and inter-event time of calving events. We find that calving events triggered by the brittle fracture of glacier ice are governed by the same power-law distributions as avalanches in the canonical Abelian sandpile model[2]. This similarity suggests that calving termini behave as self-organized critical systems that readily flip between states of sub-critical advance and super-critical retreat in response to changes in climate and geometric conditions. Observations of sudden ice-shelf collapse and tidewater glacier retreat in response to gradual warming of their environment[3] are consistent with a system fluctuating around its critical point in response to changing external forcing. We propose that self-organized criticality provides a yet unexplored framework for investigations into calving and projections of sea level rise.

Approximately 50% of mass loss from the Greenland and Antarctica ice sheets is accomplished through the calving of icebergs into the ocean, as is 40–90% of mass loss from other marine-terminating glaciers[4–6]. However, no existing parameterization or model of calving is able to reproduce observed calving rates, severely limiting the predictions made by land-ice models (for example, used in the Fifth Assessment Report of the Intergovernmental Panel on Climate Change[4,7]). We demonstrate that, similar to earthquake prediction[8], a complete and reliable model of calving must inevitably include a description of its critical nature.

We begin with a fracture model based on first principles. Fracture of a brittle material such as ice is characterized by fast crack propagation, which leads to crack branching and dense fragment formation in the fracture zones[9,10]. Driven by tension, branches radiating from the parent cracks tend to merge, creating a large number of small fragments near the parent cracks and fewer, larger fragments farther away. This process produces a power-law fragment size distribution[11] (FSD), which describes the relative abundance, $n(s)$, of fragments of size s. Eventually the crack branches run out of energy, limiting the width of the fracture zone and producing an exponential cutoff (beyond which the probability of larger fragments drops rapidly) in the FSD (ref. 11; equation (1)).

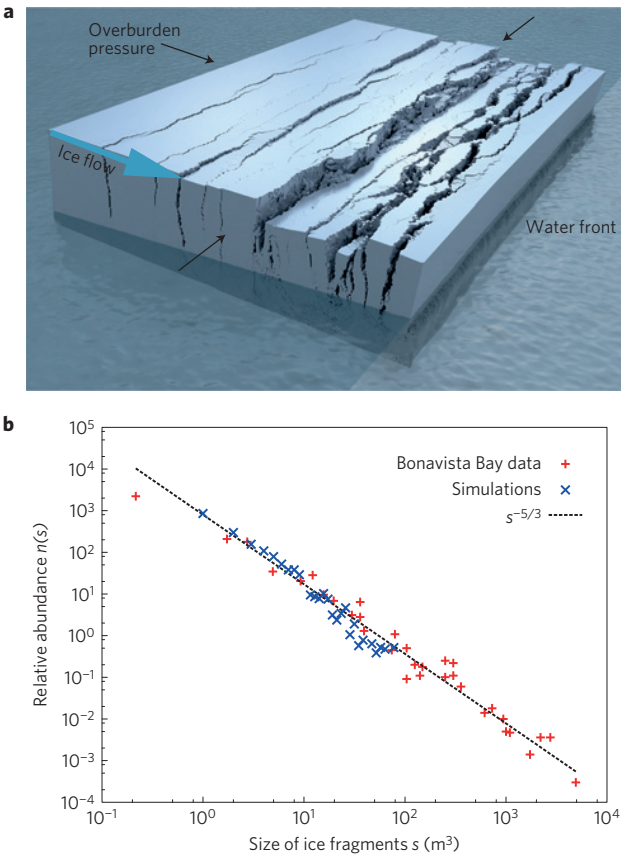

Figure 1 | Numerical model and FSD. a, Snapshot from a 3D model simulation of a 80-m-high and 500-m-long ice block terminating in 40-m-deep water supported by ice (modelled by a pressure indicated by black arrows) from three sides and open to the ocean on the fourth side. **b**, FSD resulting from model simulations, and the size distribution of ice chunks calved from icebergs in Bonavista Bay, Newfoundland[18,19]. Here, s is the volume of individual calving-debris ice chunks and $n(s)ds$ is the relative abundance in the interval ds. The line represents equation (1).

[1]CSC–IT Centre for Science, PO Box 405, 02101 Espoo, Finland, [2]Department of Earth Science, Uppsala University, Villavägen 16, 75236 Uppsala, Sweden, [3]Arctic Centre, University of Lapland, PL122, 96100 Rovaniemi, Finland, [4]Finnish Meteorological Institute, PO Box 503, 00101 Helsinki, Finland, [5]Institute of Arctic and Alpine Research, University of Colorado, Campus Box 450, Boulder, Colorado 80309, USA, [6]Alaska Science Center, US Geological Survey, 4210 University Drive, Anchorage, Alaska 99508, USA, [7]University of Texas Institute for Geophysics, 10100 Burnet Road (R2200), Austin, Texas 78758, USA, [8]State Key Laboratory of Earth Surface Processes and Resource Ecology, College of Global Change and Earth System Science, Beijing Normal University, Beijing 100875, China, [9]Department of Physics and Nanoscience Center, University of Jyväskylä, PO Box 35, 40014 Jyväskylä, Finland, [10]ITMO University, Kronverkskii ave. 49, 197101, Saint Petersburg, Russia. *e-mail: dorothee.vallot@geo.uu.se; john.moore.bnu@gmail.com

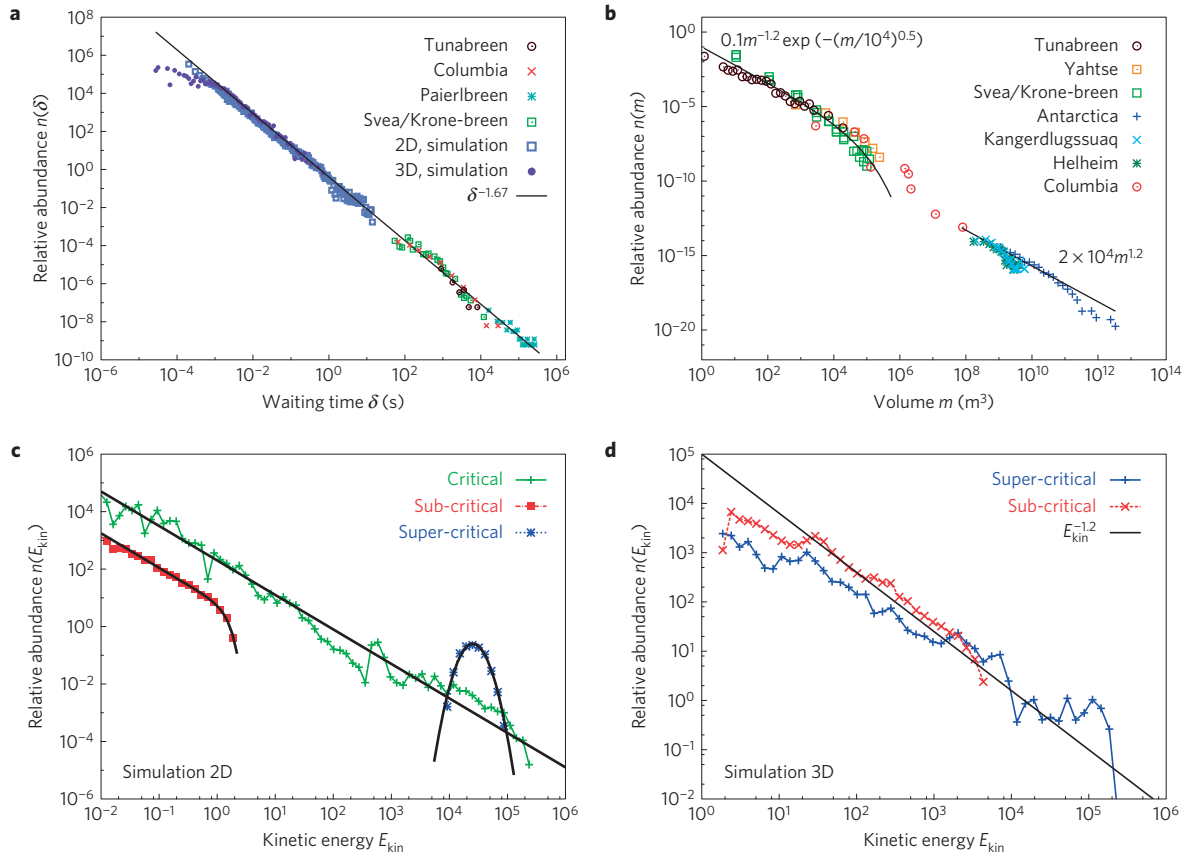

Figure 2 | Event sizes and waiting times. a, Distribution of waiting times between consecutive calving events for tidewater glaciers (Sveabreen[25] and Kronebreen[25]) and numerical simulations (ice-cliff height $H=30$ m and waterline at $H/2$). The straight line is the corresponding distribution function of the ASM model[16]. **b**, Distribution of observed calving volumes (m^3) for tidewater glaciers and ice shelves. Scaling of the data is described in Supplementary Methods 2. **c**, Distribution of kinetic energy in 2D calving simulations for critical, sub-critical and super-critical initial conditions. **d**, Distribution of kinetic energy in 3D calving simulations for near-critical sub- and super-critical initial conditions.

A calving event occurs when ice at the glacier terminus no longer has sufficient strength to support its own weight. At this point, crack propagation triggers an ice 'avalanche', a rapid burst of kinetic energy, (and corresponding loss of potential energy), that proceeds either as a falling sub-aerial mass or a rising submarine mass to the waterline. Models that describe such punctuated instabilities include the sandpile models[12], perhaps the simplest systems exhibiting self-organized criticality[2] (SOC). The hallmark of SOC is the slow, steady accumulation of an instability, eventually followed by a fast relaxation through 'avalanches' of any possible size: from a single point (for example, a $\sim$1 m^3 calving event) to system-wide collapse (the entire ice cliff collapses)[13]. In the case of glaciers, the micro-cracks and other flaws in ice, caused by its slow motion and/or ablation by water, air and solar radiation, weaken the ice until rapid fragmentation takes place, that is, a calving event. SOC systems have a sub-critical regime—distinguished by infrequent and small avalanches, allowing an instability to build up with time—and a super-critical regime—distinguished by large avalanches and widespread relaxation of the instability. They spontaneously self-organize towards a stable 'critical point' between these two unstable regimes. Close to this critical point (the 'critical region'), the system begins to exhibit scale invariance. For Abelian sandpile models (ASM), this behaviour can, to some extent, be solved explicitly[14,15]. This is manifested as pure power laws for both the mass, m, distribution of avalanches, $n(m) \propto m^{-\tau}$, and the waiting-time, δ, distribution[16] between consecutive avalanches, $n(\delta) \propto \delta^{-\sigma}$ (where τ and σ are the critical exponents of their respective distributions).

To evaluate whether SOC applies to iceberg calving, we analysed calving observations spanning 12 orders of magnitude in size from globally distributed data sets of glaciers and ice shelves (Methods and Supplementary Methods 1 and Data), and extended a recently developed numerical, particle-based calving model[17] to three dimensions (Fig. 1a and Methods and Supplementary Methods 2 and Movies). Below, we show that our calving simulations are consistent with observations and are indicative of a SOC system near its critical point. This model allows us to compare the sub-critical and super-critical calving regimes and to investigate calving's sensitivity to, for example, changes in climate.

We first consider the FSD produced in the ice-fracture process. Model results are compared to the size of ice fragments calved from icebergs in Bonavista Bay, Newfoundland[18,19]. Both observed and simulated FSDs agree with the theoretical FSD, equation (1) (Fig. 1b).

Second, we consider the distribution of waiting times between consecutive calving events from tidewater glaciers and ice shelves. Again, both the observations and the model simulations agree well with theory (Fig. 2a). The best-fit exponent for all data (both modelled and observed) is $\sigma = 1.67 \pm 0.3$, consistent with previously reported ASM findings[16].

Third, and most significantly, we consider the distribution of calving-event volumes (or equivalently, mass $\sim$ volume $\times$ 10^3, with the density of ice taken as 10^3 kg m^{-3}). Again, both observations and simulations are consistent with SOC theory (Fig. 2b–d).

Calving volume observations (Methods and Supplementary Methods 1) form two behaviourally distinct clusters (Fig. 2b). For

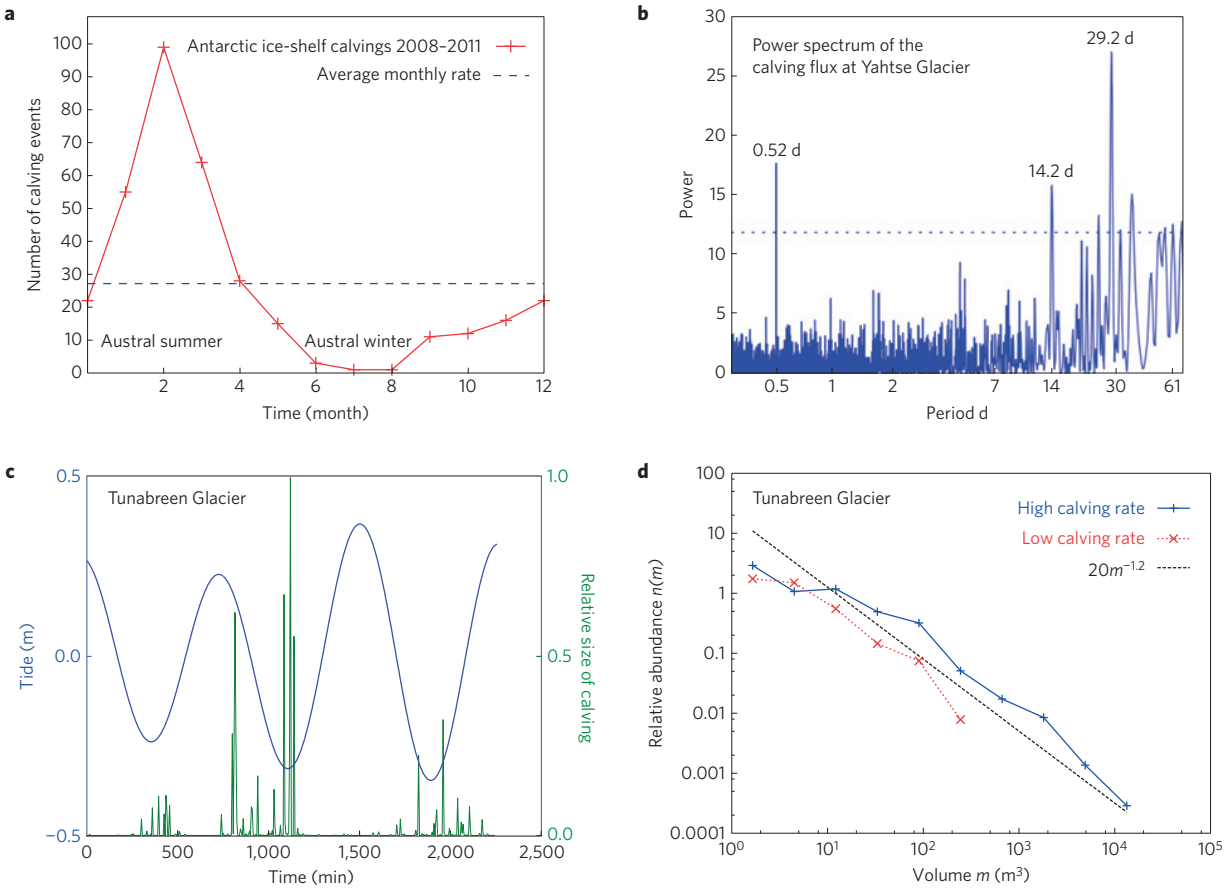

Figure 3 | Sensitivity of calving to external forcing. a, The average monthly rate of ice-shelf calving events greater than 1 km^2 in Antarctica for 2008–2011. **b**, A power spectrum of the calving flux at Yahtse Glacier, in which all of the significant periods of peak calving involve important tidal constituents. **c**, The relative calving volumes at Tunabreen over 1.7 days versus local tidal height (calculated using AOTIM-5 (ref. 26)). **d**, Distributions of the size of calving events at Tunabreen determined separately for periods of high and low calving rates, respectively. The black dashed line is the calving mass distribution, $20m^{-1.2}$.

the first group, the floating ice shelves in Antarctica and the large near-floating outlet glaciers in Greenland, calving volumes range from 10^8 to 10^{12} m^3 (as measured with satellite imagery). They are reasonably well described by a power law with exponent $\tau = 1.2$. In Antarctica, many of these events occurred, not as the release of a single large tabular iceberg, but as the sudden disintegration of the ice shelf[20] into many fragments. In contrast, for the second group, consisting of grounded tidewater glaciers in Svalbard and Alaska, calving volumes range from 10^0 to 10^5 m^3 (as inferred from either ground-based photographs or a seismic-based statistical model). They are well described by the same power law, but exhibit an exponential cutoff at $\sim 10^4$ m^3. From these results we infer that grounded calving glaciers are typically sub-critical, but approach criticality in a region near their calving margins. For grounded glaciers, the exponential cutoff of the power law reflects how calving is limited by the dimensions (width and thickness) of the terminus[21]. Columbia Glacier (red circles in Fig. 2b), bridging the two groups during a transition from a grounded to a floating terminus, suggests that a firmly grounded glacier is less prone to large-scale calving events than a floating or near-floating glacier[21,22]. Combining all calving volume data sets yields a power-law exponent of $\tau = 1.26 \pm 0.2$, a mean and range consistent with those of the different variants of the ASM (refs 14,15).

In two-dimensional (2D) simulations, sub-critical initial conditions yield small values for the kinetic energy, E_{kin}, (volume/mass proxy as explained in Methods) and a distinct exponential cutoff in the power-law distribution at $E_{kin} \sim 5$ (Fig. 2c). Criticality is characterized by strong fluctuations in E_{kin}, with a distribution approximated by a pure power law, $n(E_{kin}) \propto E_{kin}^{-1.2}$, identical to that inferred from observations (Fig. 2b). Super-criticality, meanwhile, is dominated by large events, and typically results in the failure of the entire ice cliff in a single event; $n(E_{kin})$ approximates a log-normal function with a peak around 10^4–10^5 (in units that approximate calving volume in cubic metres). As expected for a process controlled by SOC, the simulations exhibit a pure power law at the critical point and fundamentally different behaviours on either side of the critical point. Applied to the calving process, this implies that, under stable conditions, calving becomes critical (with rare large events and numerous smaller events), and even a minor climate change could induce either super-critical collapse, or increased stability (with vanishing probability for large-scale calving).

To better compare simulated and observed calving-event volumes, we repeated the simulations in three dimensions with near-critical initial conditions (Fig. 2d). As in the 2D simulations, sub-critical conditions exhibit a cutoff (at $\sim 10^3$) whereas super-critical conditions exhibit elevated (from pure power law) frequencies for the largest events (at $\sim 10^5$). These near-critical distribution functions are in agreement with those of the observations (Fig. 2b).

Next, we performed a scaling analysis of the calving-event-size distributions, $n(m)$. This reveals that the total calving rate, $\int m\, n(m)\, dm$, in the critical region (distribution function space), becomes dominated by the occurrence, or absence, of a single or a

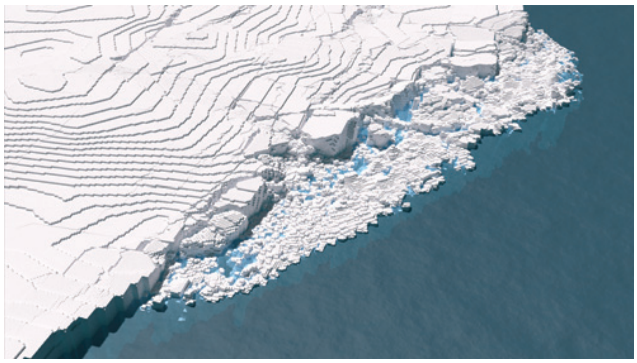

Figure 4 | Real geometry of Kronebreen, Svalbard, implemented in the particle model with a 4 m particle diameter. The entire simulation covered a 4 km^2 area at the Kronebreen calving front.

few of the largest calving events. An important implication is that fluctuations are so strong that the concept of an 'average' calving rate, as might be assumed or implemented within a large-scale ice-sheet model, is no longer meaningful[23]. Also, in the critical region, calving rate exhibits its maximum sensitivity to changes in the fracture stress of ice (Supplementary Discussion).

Our analysis thus provides strong evidence that calving exhibits the main characteristics of SOC: power-law scaling of event size and inter-event time, as well as a qualitative change in calving behaviour at the critical point. An important conclusion is that, under this framework, no calving events, no matter how large, should be considered exceptional; rather, they are samples from a scale-invariant power-law event-size distribution reflective of the critical regime. The largest possible fluctuations—spanning the size of the system itself—can occur at any time, even in the complete absence of a change in external forcing. Theoretically, a SOC system could remain forever at its critical point, but in nature, in the presence of continuously changing external forcing, the system instead fluctuates around its critical point. Such fluctuations can be observed in the seasonal variations of calving on the Antarctic ice shelves (with calving peaking in late summer and dropping off in winter, Fig. 3a) and in the tidal variations of calving at Tunabreen and Yahtse glaciers (Fig. 3b,c). The extreme sensitivity of critical systems to external forcing is highlighted at ~100-m-thick Tunabreen, where calving intensity seems to fluctuate with tidal variations of a fraction of a metre. When plotted separately for periods of low and high calving rates (Fig. 3d), these events yield distributions closely resembling the super-critical and sub-critical distributions, respectively, of the 3D simulations shown in Fig. 2d.

As the build-up of instability to the critical point is far slower than its relaxation from the super-critical state, we expect sub-critical calving (that is, dominated by small calving events) to be much more common. Only occasionally, and for relatively short periods, do calving glaciers become super-critical (that is, dominated by large-scale calving events). As observed for various ice shelves on the Antarctic Peninsula[18], centuries of stability can be followed by a retreat of the calving front to the grounding line in just a few days, again, illustrating how the concept of an 'average' calving rate can be misleading.

The intrinsically large internal fluctuations and extreme sensitivity of calving to external forcing are both inherent properties of SOC. This begins to explain why it has been so difficult to develop both practical and realistic calving parameterizations for use in large-scale, prognostic ice-flow models. We suggest that progress can be made by quantifying how environmental forcing affects the critical state of calving margins. Through observations, this may be best accomplished by monitoring changes in the probabilities of large events. Through modelling, the coupling of a 3D ice-flow model with our discrete calving model could produce realistic simulations of real glaciers (Fig. 4 and Methods and Supplementary Discussion). Constrained by observations, such simulations could help to determine how calving model parameters and thereby calving behaviour should be linked to external forcing and initial conditions and thus be used to assess the future stability and calving rates of marine-terminating glaciers worldwide.

Methods

FSD theory. Schematically, a fast-propagating crack can be assumed to branch at, more or less, regular intervals. Adjacent branches readily merge and form fragments: smaller ones near the parent crack and larger ones further from the parent crack as the branches become sparser. This process results in a power-law FSD. The crack branches run out of energy as they propagate away from the parent crack inducing an exponential cutoff in the power law and limiting the widths of the fragment zones. Such an FSD can be expressed in the form:

$$n(s) \propto s^{-\alpha} \exp(-(s/s_0)^{\eta}) + f_{\mathrm{main}}(s) \quad (1)$$

where $n(s)\mathrm{d}s$ is the relative number of fragments of size s in the size interval $[s-\mathrm{d}s/2, s+\mathrm{d}s/2]$; $\alpha=(2D-1)/D$, s_0 and η are material-, geometry- and energy-dependent parameters (where D is the dimension of the physical space). f_{main} describes the largest fragments, those formed by parent cracks merging at distances beyond the fracture zones. Fragmentation may continue following the initial break-up, through collisions or grinding of fragments (Supplementary Methods 2). The exponents of the theoretical FSD are $\alpha=5/3$ in three dimensions (Fig. 1b) and $\alpha=3/2$ in two dimensions (or $\alpha\approx1.75$ in the case of severe post-fracture break-up) as explained in Supplementary Methods 2.

Observations. Our globally distributed calving data set (Supplementary Information: Calving Event Catalogue, Supplementary Data) lists the waiting times and sizes of calving events in Alaska, Greenland, Svalbard and Antarctica. As the methods of observation vary between study sites, rescaling is necessary for comparison. Columbia and Yahtse tidewater glaciers in Alaska were observed with photogrammetric or seismic methods. Tunabreen, Paierlbreen, Kronebreen and Sveabreen tidewater glaciers in Svalbard were observed directly or with photogrammetric methods. Helheim and Kangerdlugssuaq outlet glaciers in Greenland and all large Antarctic ice shelves (larger than 10 km^2) were monitored with satellite imagery. The study sites form two clusters: the smaller, field-observed tidewater glaciers and the larger, satellite-observed glaciers and ice shelves. The distribution functions for Tunabreen and the Greenland glaciers, chosen as standards for each group, are normalized per 30 s of observation and per 1 km of terminus width. We rescaled the average calving intensities of the remaining glaciers to match the calving intensities of their respective categories. Here rescaling means $n(m) \rightarrow n(m)/a$ with $n(m)$ being the relative abundance of events for a given volume, m, and a glacier-dependent constant, a. Field and remote sensing methods are described in detail in Supplementary Methods 1.

Simulations. Our numerical analyses are based on a 3D extension of a 2D particle-based model[17]. In the simulation model, a glacier is divided into discrete particles, approximately 1 m^3 in size. Initially these particles are densely packed and partly frozen together. Frozen contacts are modelled as beams that break as their elastic loads exceed a predefined fracture threshold. Trajectories of the ice particles are solved iteratively from an initial geometry and a set of initial conditions. Particles interact inelastically, which means that their mutual collisions dissipate energy. Calving events are identified as peaks in the total time-dependent kinetic energy E_{kin} that evolves with time. The waiting time between events is measured as the time elapsed between subsequent breakings of beams. Fragment sizes are defined as the number of particles in clusters connected by unbroken beams.

The distribution of E_{kin} provides a normalized proxy for the distribution of calving mass or volume (Fig. 2c,d): only particles undergoing calving have enough velocity to significantly contribute to the total kinetic energy. Calved particles reach velocities, v_i, of the order of 1–10 m s^{-1}, more or less independent of the calved mass, hence the distribution $\Sigma_i 1/2 m_i v_i^2$ should, after rescaling, have a similar distribution function as the mass (or the volume) of a calving event, $\Sigma_i m_i$.

The fracture stress, σ_c, of the model ice is used as a tuning parameter to change between criticality regimes. Changing this parameter is rather crude but represents a simple way to model, for example, the weakening of ice as a result of partial melting or micro-fracturing. In more detailed projections, changes in the terminus geometry of a glacier (that is, sea level, ice thickness and so on), would also induce changes in criticality. This is explained in more detail in Supplementary Methods 2.

Coupling of the calving model to a glacier-flow model. We couple our calving model to a large-scale ice-flow model by alternating runs of our discrete, particle-based calving simulations and the continuum ice-flow model Elmer/Ice[24]. The ice geometry in the expected calving region is extracted from the flow model and serves as an initial condition for the calving model. Calving events subsequently alter the glacier geometry, which feeds back on the continuum model. Simulations from a synthetic small-scale example and 4 km^2 of the Kronebreen calving front are presented in the Supplementary Discussion.

Sources of the data used. All individual calving-event times and volumes used to derive the statistical distributions presented in this study have been archived in a common format (Supplementary Information: Calving Event Catalogue, Supplementary Data).

Received 4 June 2014; accepted 9 October 2014; published online 10 November 2014

References

1. Moore, J. C., Grinsted, A., Zwinger, T. & Jevrejeva, S. Semi-empirical and process-based global sea level projections. *Rev. Geophys.* **51,** 484–522 (2013).
2. Bak, P., Tang, C. & Wiesenfeld, K. Self-organized criticality: An explanation of the 1/f noise. *Phys. Rev. Lett.* **59,** 381–384 (1987).
3. Luckman, A., Murray, T., de Lange, R. & Hanna, E. Rapid and synchronous ice-dynamic changes in East Greenland. *Geophys. Res. Lett.* **33,** L03503 (2006).
4. Anthoff, D., Nicholls, R. J., Tol, R. S. J. & Vafeidis, A. T. *Global and Regional Exposure to Large Rises in Sea-Level: A Sensitivity Analysis* (Tyndall Centre for Climate Change Research, 2006).
5. Rignot, E., Velicogna, I., van den Broeke, M. R., Monaghan, A. & Lenaerts, J. Acceleration of the contribution of the Greenland and Antarctic ice sheets to sea level rise. *Geophys. Res. Lett.* **38,** 1–5 (2011).
6. Rignot, E., Jacobs, S., Mouginot, J. & Scheuchl, B. Ice-shelf melting around Antarctica. *Science* **341,** 266–270 (2013).
7. Bindschadler, R. A. *et al.* Ice-sheet model sensitivities to environmental forcing and their use in projecting future sea level (the SeaRISE project). *J. Glaciol.* **59,** 195–224 (2013).
8. Main, I. Is the reliable prediction of individual earthquakes a realistic scientific goal? *Nature Debates* http://www.nature.com/nature/debates/earthquake (1999).
9. Fineberg, J. & Marder, M. Instability in dynamic fracture. *Phys. Rep.* **313,** 2–108 (1999).
10. Åström, J. A. Statistical models of brittle fragmentation. *Adv. Phys.* **55,** 247–278 (2006).
11. Kekäläinen, P., Åström, J. A. & Timonen, J. Solution for the fragment-size distribution in a crack-branching model of fragmentation. *Phys. Rev. E* **76,** 026112 (2007).
12. Bak, P. *How Nature Works: The Science of Self-Organized Criticality* (Springer, 1996).
13. Jensen, H. J. *Self-Organized Criticality* (Cambridge Univ. Press, 1998).
14. Dhar, D. The Abelian sandpile and related models. *Physica A* **263,** 4–25 (1999).
15. Dhar, D. Theoretical studies of self-organized criticality. *Physica A* **369,** 29–70 (2006).
16. Paczuski, M., Boettcher, S. & Baiesi, M. Interoccurrence times in the Bak–Tang–Wiesenfeld sandpile model: A comparison with the observed statistics of solar flares. *Phys. Rev. Lett.* **95,** 181102–181105 (2005).
17. Åström, J. A. *et al.* A particle based simulation model for glacier dynamics. *Cryosphere* **7,** 1591–1602 (2013).
18. Crocker, G. B. Size distributions of bergy bits and growlers calved from deteriorating icebergs. *Cold Reg. Sci. Technol.* **22,** 113–119 (1993).
19. Savage, S. B., Crocker, G. B., Sayed, M. & Carriers, T. Size distribution of small ice pieces calved from icebergs. *Cold Reg. Sci. Technol.* **31,** 163–172 (2000).
20. Scambos, T. A., Hulbe, C. L. & Fahnestock, M. A. Climate-induced ice shelf disintegration in the Antarctic Peninsula. *Antarct. Res. Ser.* **79,** 79–92 (2003).
21. Bassis, J. N. & Jacobs, S. Diverse calving patterns linked to glacier geometry. *Nature Geosci.* **6,** 833–836 (2013).
22. Amundson, J. A. & Truffer, M. A unifying framework for iceberg-calving models. *J. Glaciol.* **56,** 822–830 (2010).
23. Bassis, J. N. The statistical physics of iceberg calving and the emergence of universal calving laws. *J. Glaciol.* **57,** 3–16 (2011).
24. Gagliardini, O. *et al.* Capabilities and performance of Elmer/Ice, a new-generation ice sheet model. *Geosci. Model Dev.* **6,** 1299–1318 (2013).
25. Chapuis, A. & Tetzlaff, T. The variability of tidewater-glacier calving: Origin of event-size and interval distributions. *J. Glaciol.* **60,** 622–634 (2014).
26. Padman, L. & Erofeeva, S. A. Barotropic inverse tidal model for the Arctic Ocean. *Geophys. Res. Lett.* **31,** L02303 (2004).

Acknowledgements

We thank J. A. Jania, D. Ignatiuk, M. Laska, B. Luks, M. Ciepły, J. Halat, A. Piechota, M. Sund and crews from the Polish Polar Station in Hornsund (Institute of Geophysics, Polish Academy of Sciences) for their help collecting data at Paierlbreen; A. Hodson and D. Benn for their help at Tunabreen; and G. Hamilton for suggesting the Greenland data. Kronebreen geometry was provided by the Norwegian Polar Institute. The European Space Agency provided ENVISAT ASAR imagery for the Antarctic ice shelves. Support provided by: SvalGlac (Paierlbreen); SVALI (Tunabreen); US Geological Survey Climate and Land Use Change, Department of Interior Climate Science Center, and Prince William Sound Regional Citizens' Advisory Council (Columbia Glacier); NSF-EAR-0810313 (Yahtse Glacier); National Basic Research Program of China (2012CB957704 and 2015CB953600) and Fundamental Research Funds for the Central Universities of China (2013NT5) (Antarctic ice shelves). This publication is contribution number 33 of the Nordic Centre of Excellence SVALI, 'Stability and Variations of Arctic Land Ice', funded by the Nordic Top-level Research Initiative (TRI).

Author contributions

J.A.Å. and T.I.R. constructed the calving model. J.A.Å. assembled and interpreted the calving observations. Co-authors collected, processed or interpreted the calving observations, as follows: Columbia (E.Z.W. and S.O'.N.), Yahtse (T.C.B. and S.O'.N.), Tunabreen (D.V.), Paierlbreen (M.S. and E.Z.W.), Helheim and Kangerdlugssuaq (M.S.), and Antarctic ice shelves (Y.L. and J.C.M.). T.Z. performed the ice-flow model simulations. E.Z.W. compiled the Calving Event Catalogue. All authors have contributed to, seen and approved the manuscript.

Additional information

Supplementary information is available in the online version of the paper. Reprints and permissions information is available online at www.nature.com/reprints. Correspondence and requests for materials should be addressed to D.V. or J.C.M.

Competing financial interests

The authors declare no competing financial interests.